Bilecik Şeyh Edebali Üniversitesi Fen Bilimleri Dergisi
Bilecik Seyh Edebali University Journal of Science
12(1), 47-59, 2025
DOİ: 10.35193/bseufbd.1433327
e-ISSN: 2458-7575 (https://dergipark.org.tr/tr/pub/bseufbd)

Araştırma Makalesi – Research Article

Investigation of the Flow Characteristics of the Compression Ring Groove Cavity in the Expansion Time of a Compression Ignition Engine

Sıkıştırma ile Ateşlemeli Bir Motorun Genişleme Zamanında Kompresyon Segman Yuvası Boşluğunun Akış Karakteristiklerinin İncelenmesi

Emrah Kantaroğlu[1*]

Geliş / Received: 07/02/2024 ***Revize / Revised: 13/03/2024*** ***Kabul / Accepted: 20/03/2024***

ABSTRACT

In the expansion stroke of reciprocating engines, it is desired that the pressure generated after combustion acts on the piston surface without any losses. However, there are some losses during this process. One of these is the pressure losses in the ring grooves and gaps. In this study, the flow characteristics of the peak compression ring gaps of the Renault F8Q706 engine were examined. Investigations were carried out using Computational Fluid Dynamics (CFD) at 2500 rpm, full load and at the beginning of the piston expansion stroke after a crankshaft angle of 15 from the top dead center. Combustion products were used as fluids in the investigations. In the study, firstly, a 1D engine model was created and verified with the same engine tests in the literature. In-cylinder characteristics taken from the 1D model are defined as boundary conditions in 2-Dimensional (2D) CFD analyses. As a result, in response to the ring cavity inlet pressures of 6.5MPa, 5MPa, 3MPa, the leakage flow rates in the cavity were calculated as 2.97E-05, 1.66E-05, 3.41E-6 kg/s, respectively. For 6.5 MPa inlet pressure, the net pressure was calculated as 6.49941 MPa as a result of the pressure losses in the ring gap.

Keywords- CFD, piston Ring, Sealing

ÖZ

Pistonlu motorların güç strokunda, yanma sonu oluşan basıncın kayıpsız olarak piston yüzeyine etkimesi istenir. Ancak yaşanan kayıplardan bir tanesi segman yuvalarındaki ve boşluklarındaki basınç kayıplarıdır. Bu çalışmada, Renault F8Q706 motorunun tepe kompresyon segmanı boşluğunun akış özellikleri incelenmiştir. İncelemeler, Hesaplamalı Akışkanlar Dinamiği (HAD) analizi kullanılarak 2500 d/dk'de, tam yükte ve üst ölü noktadan 15° krank mili açısı sonrasındaki güç strokunda yapılmıştır. Akışkan olarak yanma sonu ürünleri kullanılmıştır. Öncelikle 1-Boyutlu (1B) motor modeli oluşturulmuş ve literatür testleri ile doğrulanmıştır. 1B modelden alınan silindir içi karakteristikler 2-Boyutlu (2B) HAD modelinde tanımlanmıştır. Sonuçta, 6,5MPa, 5MPa, 3MPa giriş basınçlarında, kaçak debiler sırasıyla 2,97E-05, 1,66E-05, 3,41E-6 kg/s olarak hesaplanmıştır. 6,5 MPa giriş basıncı için, segman boşluğunda oluşan basınç kayıpları sonunda net basınç 6.49941 MPa olarak hesaplanmıştır.

Anahtar Kelimeler- HAD, Segman, Sızdırmazlık

[1]*Corresponding Author Contact: emrahkantaroglu@kku.edu.tr (https://orcid.org/0000-0002-6127-4318)
Kırıkkale University, Faculty of Engineering and Natural Sciences, Department of Mechanical Engineering, Kırıkkale

I. INTRODUCTION

While internal combustion engines are still advantageous in terms of high power and range, their usage is decreasing due to growing environmental concerns. The environmental issues primarily stem from toxic emissions and greenhouse gas effects resulting from the combustion of hydrocarbon fuels. In addition to these environmental issues, rising costs due to decreasing oil reserves are also a factor. Therefore, in engine development, the primary focus is on achieving the highest efficiency and minimizing emissions.

Efficiency is an evolving concept in internal combustion engines. Combustion losses, heat transfer losses, friction losses, and pumping losses reduce the efficiency of these engines to around 30%. Despite ongoing fuel searches to overcome these efficiency losses, the existing mechanics of engines continue to contribute to these losses. Due to the disadvantages associated with power generation in internal combustion engines, the advancement of digital technologies and electric infrastructure has shifted the trend towards electric motors in transportation. This has begun to restrict the use of internal combustion engines in transportation, and electric motor technologies providing an alternative means of transportation have become widespread.

Many developed countries worldwide have announced their intentions to phase out diesel fuel usage and ban the sale of vehicles with internal combustion engines by 2035. Türkiye, through the Paris Agreement, has declared its commitment to complete this transition between 2030 and 2050 [1]. According to the September 2024 data from the Turkish Statistical Institute (TÜİK), 1.3% of the 14,967,044 automobiles in Turkey are hybrid, and 0.3% are fully electric. There are still 14,727,572 automobiles equipped with internal combustion engines [2]. While the origin of this trend appears to be high efficiency and emission constraints, current battery technologies and stable power delivery are still considered limiting factors for electric motors. Compression Ignition (CI) engines continue to play a crucial role in heavy-duty transportation services and electricity generation transformations, where electric motors are not yet able to respond. Therefore, the use of compression-ignition engines persists with new fuel and engine technologies that mitigate emission releases [3-4]. The effective achievement of compression end pressure without loss and the preservation of the reached pressure during the power period are crucial for preventing efficiency losses. In engines, internal losses within the cylinder can be attributed to fuel, combustion, and flow, as well as thermal loads. In the literature, the efficiency losses caused by thermal loads in engines have been investigated both experimentally and numerically [5]. Piston rings are used to prevent losses in the cylinder and balance the movement of the piston [6]. These rings, located in the upper section of the piston during compression and expansion stroke, ensure that high-pressure air does not escape to the lower section, thus preventing pressure loss. Simultaneously, these rings also function as sealing elements. Comas et al. [7] emphasized the significance of sealing efficiency and developed analyses incorporating the dynamic behaviors, tribological characteristics, and gas leakage conditions of the compression ring. Lozano et al. [8] investigated flow losses in compression rings using CFD simulations and mathematical models. Koszalka [9] simulated the effects of selected dimensions of the rings and piston of a diesel engine on performance. The results have shown that with restrictions imposed by the engine manufacturer regarding the scope of modernization, it is possible to significantly reduce or even eliminate the reverse gas flow from the inter-ring space to the combustion chamber. In his study on piston rings, Yeşilada [10] examined the wear, breakage and irregular movement of the rings. The study emphasized the critical role of rings in internal combustion engines and emphasized that rings are an important factor affecting engine performance. Chucholowski et al. [11] and Kornprobst et al. [12] developed the first 2D simulation model for the entire piston-cylinder assembly. Their work involved calculating horizontal film thickness and hydrodynamic friction, considering piston dynamics, piston ring dynamics, and gas dynamics. They described the interaction between rings and piston grooves using analytical equations. Furuhama et al. [13] conducted theoretical and experimental studies on gas transport in ring cavity clearances. Karamangil [14] developed thermodynamic models for combustion chamber gases and numerical models for hydrocarbons in the ring, finding that hydrocarbons in the ring groove took longer to leave the cylinder after the combustion event. In their study, Lyubarskyy and Bartel [15] created a 2D CFD model for the piston rings of a diesel-fueled engine. Analyzing mass flow along the ring cavity, they examined pressure and fluid friction, discovering increased flow losses in ring cavity clearances with rising average pressure.

In the literature, there are limited studies on the flow characteristics of clearances in ring cavities, particularly for expansion or power periods. Therefore, there is insufficient research to ensure the highest possible occurrence or examination of the spreading load created by the high pressure generated after combustion on the piston. In this study, a Renault F-Type F8Q706 engine was disassembled. Subsequently, a 1D engine model was created by taking measurements of the manifold, port, valve, cylinder, combustion chamber, and block. Using the obtained measurements and the cylinder characteristics from the 1D engine model, a 2D ring cavity geometry model was created and analyzed. The study examined pressure loss and leakage flows from the ring cavity during the expansion time after combustion.

II. MATERIAL AND METHOD

In this study, the Renault F8Q706 engine was initially modelled as a 1D model in the Ricardo-Wave software to examine the flow characteristics in the ring cavity during the expansion stroke. After verifying the 1D engine model analyses with test results available in the literature, the obtained in-cylinder pressure and temperatures during the expansion stroke were utilized as boundary conditions for the 2D ring cavity analysis. Additionally, the mass fractions of gases inside the cylinder under theoretical complete combustion conditions were calculated to define the fluid type in the 2D ring cavity model.

A. 1D Engine Model Analysis

In this study, the 1D engine model was developed using the Ricardo-WAVE 2019.1 software. Various sub-models were employed in the 1D engine model, including flow friction, turbulence, heat transfer, combustion, and emission models. The 1D engine model utilized geometric and physical dimensions from all components of the engine [16]. The engine and piston dimensions for the F8Q706 model are provided in Table 1 and Table 2. The geometries used in the Wave software are as follows:

The Woschni heat transfer model was defined for the heat transfer model [17].

The Diesel-Wiebe model was used for the turbulent combustion model [18-19].

For the formation of CO and CO_2 emissions, the Newhall model was applied [20], Cheng model for unburned HC emissions [21], Fenimore model for NO_x [22], and Heywood correlations were used [22].

The Chen-Flynn correlation model was employed for mechanical friction losses [23].

The software was configured with a diesel fuel definition, and 250 engine cycles were simulated to ensure steady-state conditions. A time step of 0.1s and a convergence criterion of 0.001 were defined. Figure 1 illustrates the model geometry and valve profiles, and Table 3 provides the boundary conditions defined in the software [8, 12, 21].

Table 1. Main specifications of engine [16].

Engine Model	Renault F-Type F8Q 706
Number of cylinders	4
Displacement, cc	1870
Bore, m	0.08
Stroke, m	0.093
Compression ratio	21.5: 1
Max. torque, Nm at 2500 rpm	118
Max. power, kW at 4500 rpm	47

Table 2. Fuel properties [24]

Properties of Diesel Fuel	Quantity
Chemical Formula	$C_{12}H_{23}$
Lower heating value, MJ/kg	43.1
H/C ratio	1.92
Density, kg/m^3	835
Stoichiometric	14.6
Flash point, K	330
Boiling point, K	633

Table 3. Temperature and pressure values on boundary surfaces. (1D model) [25, 26, 27, 28].

Boundary Surfaces	Pressure (Bar)	Temperature (K)
Inlet (Air)	2.56	327.5
Outlet (Burned gases)	2.83	904
Piston	-	595
Intake port	-	323
Exhaust port	-	490
Liner	-	616
Head	-	635
Intake valve	-	345
Exhaust valve	-	500

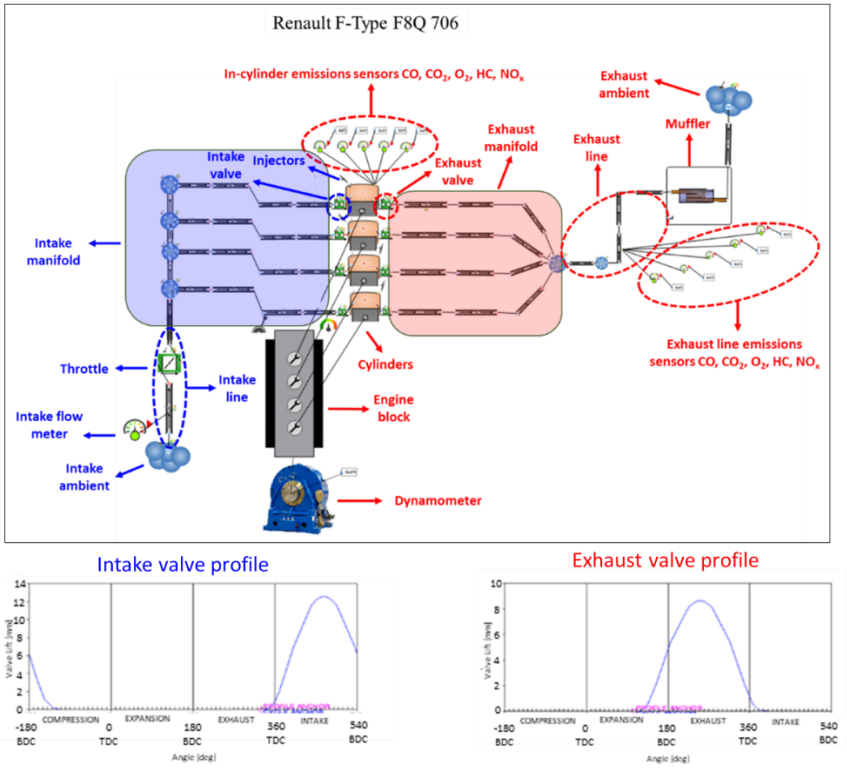

Figure 1. 1D Model and valve profiles.

The 1D engine model for the Renault F8Q706 engine was validated by comparing it with catalog data and literature, as shown in Figure 2. As observed, the power variation trends are similar in all three evaluations. [16, 29]. Upon examining Figure 2, it is observed that the power values obtained from the 1D engine model are respectively 8.526%, 8.555%, 7.596%, and 8.965% higher than the test values in the literature for engine speeds of 1,000, 2,000, 3,000, and 4,000 rpm. Additionally, the power obtained from the 1D engine model is 8.785% higher at 2,500 rpm and 9.457% higher at 4,500 rpm compared to the catalogue power values [29].

These differences arise due to variations in test conditions and modeling conditions. Differences in fuel content, ambient air composition, ambient air temperature/pressure, and variations created by the ideal engine operation are common factors causing such discrepancies in engine modeling. Despite these variations, the 1D model was implemented to apply test conditions as accurately as possible. In the 1D modeling, at the engine's maximum torque speed of 2,500 rpm and full load conditions, the gas temperature and pressure inside the cylinder were calculated during the expansion phase, 15 degrees after the top dead center (ATDC). These values are presented in Table 4.

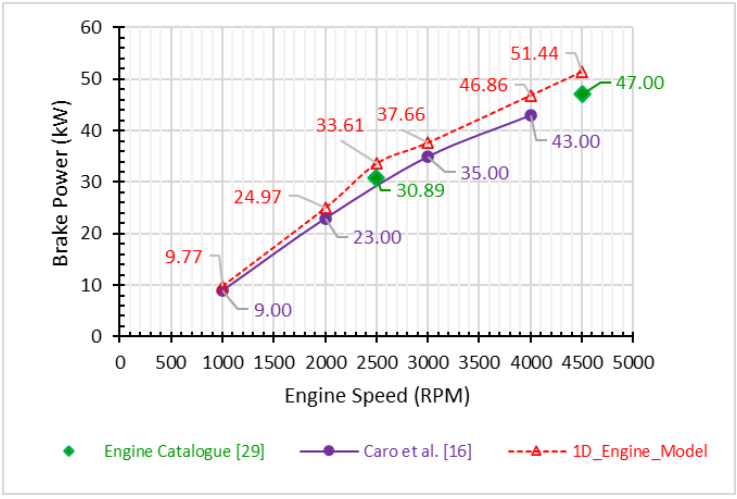

Figure 2. 1D engine model calibration and validation.

Table 4. In-cylinder parameters calculated from the 1D engine model.

In-Cylinder Measurements (after TDC 15KMA)	Quantity
Max. pressure, MPa	6.5
Max. temperature, K	1 888

B. 2D Ring Cavity CFD Model

CFD analyses involve numerical solutions for thermal-fluid problems. In these analyses, a mesh structure is applied to the region bounded by all surfaces involved in the geometry for the inlet and outlet. Conservation equations are then solved at the intersection points of this mesh structure. These equations are mass, momentum, and energy conservation equations. The solutions in CFD models can be either time-dependent or time-independent, and they may encompass static and dynamic flow models. The construction of CFD analyses involves pre-processing, solver, and post-processing. Figure 3 illustrates the steps taken in this study.

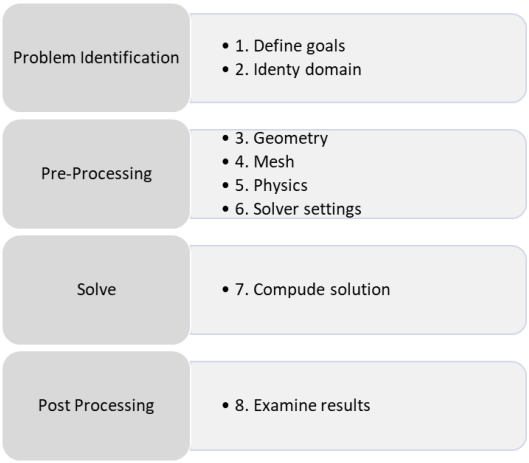

Figure 3. CFD model process.

During the flow, fluid particles are subjected to gravitational, inertial, pressure, and friction forces. These forces induce changes in the velocity of fluid particles. Similarly, heat fluxes resulting from heat transfer between the fluid and its surroundings also cause temperature changes in fluid particles. The Reynolds transport theorem (mass, energy, momentum conservation) is applied to each fluid particle (differential element) in all axes of the fluid, and the numerical solution to the complex equations without analytical solutions is obtained through the Finite Difference Method. The conservation equations for the differential elements within the model are solved using these equations to reach a conclusion.

The conservation of mass is shown in Equation 1.

$$\rho\vec{\nabla}.\vec{V} = \rho\left(\frac{\partial u}{\partial x}+\frac{\partial v}{\partial y}+\frac{\partial w}{\partial z}\right) \tag{1}$$

The continuity equation, in vector form, is written as in Equation 2.

$$\frac{D\rho}{Dt}+\rho\vec{\nabla}.\vec{V}=0 \tag{2}$$

In Cartesian coordinates, momentum conservation, based on Newton's second law of motion, is given in Equation 3.

$$\rho\frac{D\vec{V}}{Dt}=\vec{f}-\vec{\nabla}P+\mu\nabla^2\vec{V} \tag{3}$$

In Cartesian coordinates, when the first law of thermodynamics is applied Equation 4 is obtained in vector form:

$$\frac{DT}{Dt}=\alpha\nabla^2T+\frac{q'}{\rho c_p} \tag{4}$$

The case where viscous heat generation is not neglected is represented by Equation 5:

$$\frac{DT}{Dt}=\alpha\nabla^2T+\frac{q'}{\rho c_p}+\frac{\Phi}{\rho c_p} \tag{5}$$

The continuity equation used in ANSYS-Fluent CFD analyses is shown in Equation 6.

$$\frac{\partial \bar{\rho}_k}{\partial t} + \nabla.(\bar{\rho}_k \tilde{u}) = \nabla.\left[\bar{\rho} D_T \nabla\left(\frac{\bar{\rho}_k}{\bar{\rho}}\right)\right] + \dot{\rho}^c{}_k + \dot{\rho}^s{}_k \qquad \text{(k=1,.....K)} \tag{6}$$

Equation 7 shows the momentum conservation equation used in ANSYS-Fluent CFD analyses.

$$\frac{\partial \bar{\rho}\tilde{u}}{\partial t} + \nabla.(\bar{\rho}\tilde{u}\tilde{u}) = -\nabla\bar{\rho} + \nabla.\bar{\sigma} - \frac{2}{3}\bar{\rho}\tilde{k}l + \overline{F}^s + \overline{\rho g} \tag{7}$$

Equation 8 displays the energy conservation equation used in ANSYS-Fluent CFD analyses.

$$\frac{\partial \bar{\rho}\tilde{I}}{\partial t} + \nabla.(\bar{\rho}\tilde{u}\tilde{I}) = -\bar{\rho}\nabla\tilde{u} + \nabla\tilde{J} + \bar{\rho}\tilde{\varepsilon} + \dot{\bar{Q}}^c + \dot{\bar{Q}}^s \tag{8}$$

Equations 9 and 10 represent the Reynolds-Averaged Navier-Stokes (RANS) equations for k and ε used in ANSYS-Fluent CFD analyses.

$$\frac{\partial \bar{\rho}\tilde{k}}{\partial t} + \nabla.(\bar{\rho}\tilde{u}\tilde{k}) = -\bar{\rho}\tilde{k}\nabla.\tilde{u} + \sigma:\nabla\tilde{u} + \nabla.\left[\frac{(\mu+\mu_T)}{Pr_\varepsilon}\nabla\tilde{k}\right] - \bar{\rho}\tilde{\varepsilon} + \dot{\bar{W}}^s \tag{9}$$

$$\frac{\partial \bar{\rho}\tilde{\varepsilon}}{\partial t} + \nabla.(\bar{\rho}\tilde{u}\tilde{\varepsilon}) = -\left(\frac{2}{3}c_{\varepsilon 1} - c_{\varepsilon 3}\right)\bar{\rho}\tilde{\varepsilon}\nabla.\tilde{u} + \nabla.\left[\frac{(\mu+\mu_T)}{Pr_\varepsilon}\nabla\tilde{\varepsilon}\right] - \frac{\tilde{\varepsilon}}{\tilde{k}}\left(c_{\varepsilon 1}\sigma:\nabla\tilde{u} - c_{\varepsilon 2}\bar{\rho}\tilde{\varepsilon} + c_s\dot{\bar{W}}^s\right) \tag{10}$$

The RNG (ReNormalization Group) model for the turbulent dissipation rate (ε) is given by Equation 11:

$$\frac{\partial \bar{\rho}\tilde{\varepsilon}}{\partial t} + \nabla.(\bar{\rho}\tilde{u}\tilde{\varepsilon}) = -\left(\frac{2}{3}c_{\varepsilon 1} - c_{\varepsilon 3}\right)\bar{\rho}\tilde{\varepsilon}\nabla.\tilde{u} + \nabla.\left[\frac{(\mu+\mu_T)}{Pr_\varepsilon}\nabla\tilde{\varepsilon}\right] - \frac{\tilde{\varepsilon}}{\tilde{k}}\left(c_{\varepsilon 1}\sigma:\nabla\tilde{u} - c_{\varepsilon 2}\bar{\rho}\tilde{\varepsilon} + c_s\dot{\bar{W}}^s\right) - \bar{\rho}R \tag{11}$$

C. Geometry

This study conducted a 2D ring cavity analysis for the expansion phase using the ANSYS-Fluent 2023 R1 module. Therefore, the ring cavity geometry was designed in 2D. The data obtained after the Renault F-Type F8Q706 engine disassembled, as shown in Figure 4, were used to define the geometric measurements using Tables 1 and 5. The surface representation of the 2D ring cavity geometry was created using the SolidWorks software package. When creating the model file in ANSYS-Fluent, the fluid surface was drawn as a solid surface and defined as a fluid. While the piston was at expansion stroke, the flow in the top ring, which is the examination region, was examined by taking the in-cylinder parameters taken from the 1D model. Lozano et al. [8] stated in their study that during the movements of the piston, the ring in the groove does not move smoothly and is in different positions. This limits the flow losses. Even if a smooth movement is displayed as in Mohamed [6]'s study and the ring fits snugly to the ceiling of the slot (for expansion stroke), the flow losses will still be limited. The ring in this study was positioned considering the ideal situation where the ring is in the middle and does not sit on a surface, which is the situation where the highest loss is experienced in terms of flow losses. Figure 5 provides the nomenclature of the surfaces and regions used in the 2D CFD analyses for the ring cavity.

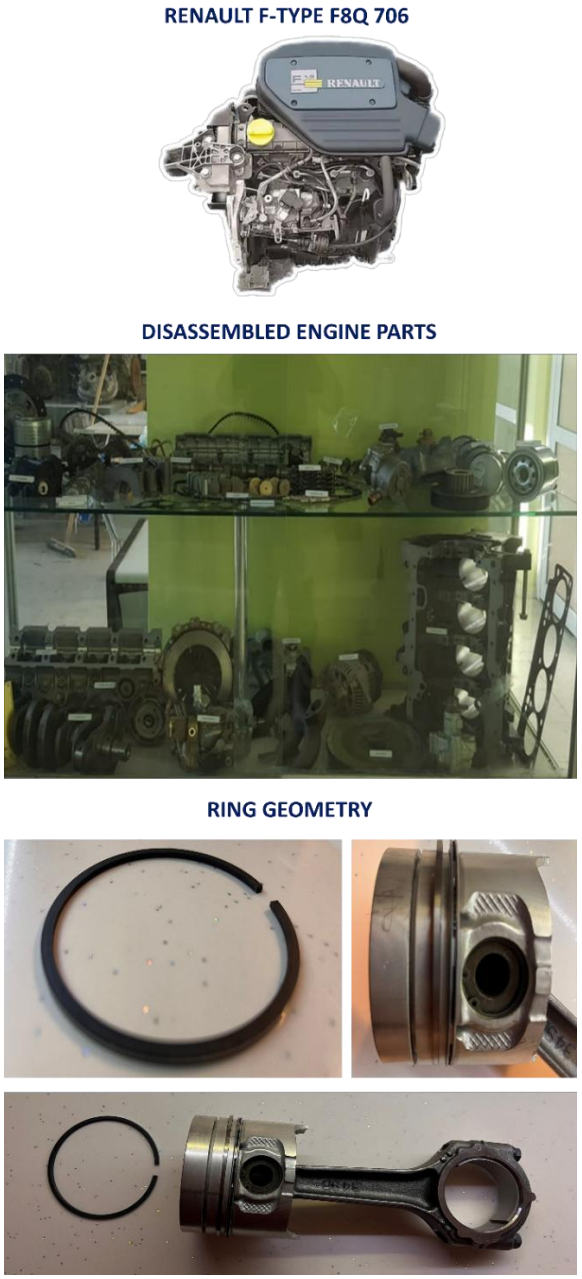

Figure 4. Engine, piston, and ring images.

Table 5. Piston dimensions and characteristics.

Piston Parameter	**Length (mm)**
Compression Height	42.25
Combustion Chamber Depth	0.7
Full Length	70.5
Piston Firing Kit Dimension	12.5
Pin Length	63
Pin Diameter	24
1st Ring Axial Height	2
2nd Ring Axial Height	2
3rd Ring Axial Height	3

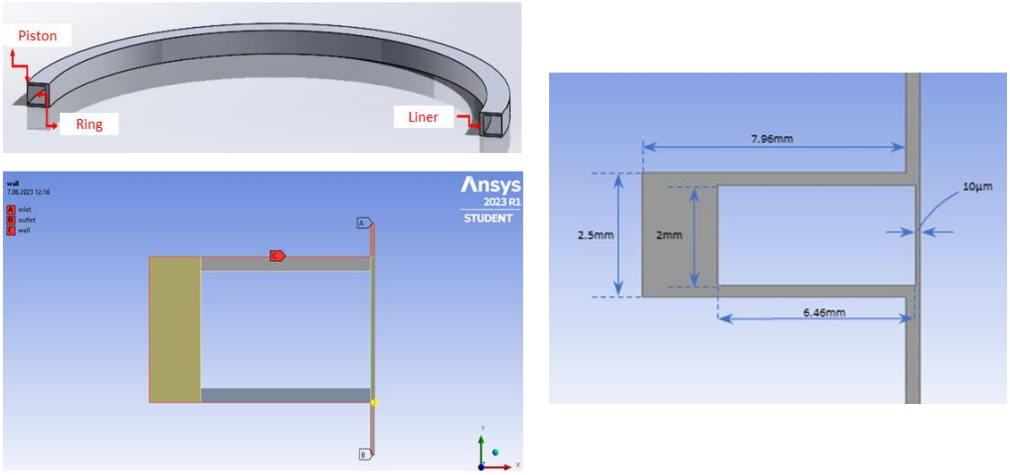

Figure 5. CFD model.

D. Mesh Structure

Specific partial differential equations are solved at the intersection points of the mesh structures created in geometry. Therefore, the mesh structure is important in reflecting the model's reality, including its number and density. Mesh structures can be in different numbers, geometries, and sizes. It relies on experimental and analytical methods for its selection. The mesh structure used in this study was created using ANSYS-Workbench. In the mesh structure definitions, the aspect ratio was taken between 1 and 2, and skewness was set to be less than 0.9. When creating the mesh structure, only the element size definition was made on the geometry, with the element size value set to 0.001 mm. Additionally, inflation definitions were made for the inlet edge, cylinder liner surface (piston wall), engine body surface (liner wall), and outlet. The current mesh structure has a total element count of 924,698. Figure 6 shows the created mesh structure.

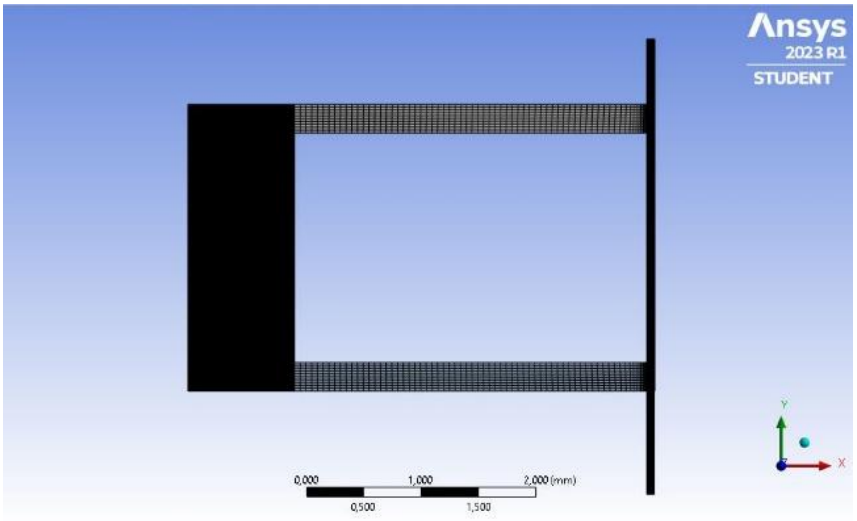

Figure 6. Mesh structure.

The mesh independence test is conducted to evaluate how the results of an analysis are influenced by the number of meshes used. This test involves comparing the results obtained by repeating the same analysis with different mesh counts. The aim is to assess the degree to which the analysis outcomes are affected by the number of meshes used.

To demonstrate the independence of the leakage flow results from the mesh count, repetitive analyses were conducted at 6.5 MPa with different mesh counts. These analyses were performed at an engine speed of 2500 rpm, at full load, in a steady-state, and during the expansion phase. Mesh independence tests conducted within the scope of this study are presented in Figure 7. When examining leakage flows based on mesh counts, it is evident that the most stable and effective mesh count is 924,698.

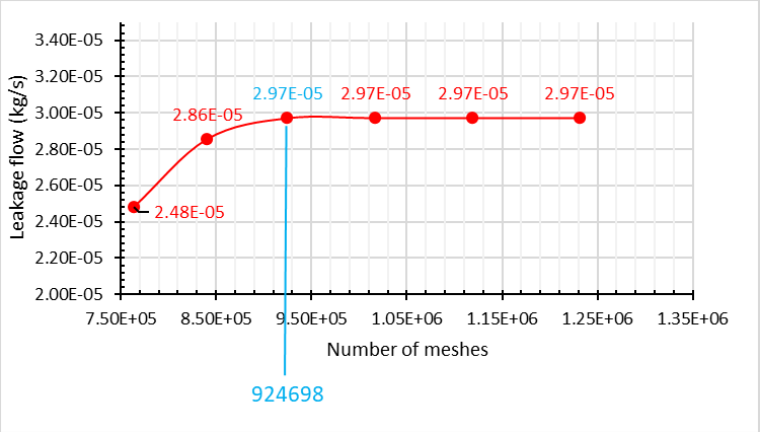

Figure 7. Mesh independence test.

E. Model Definitions

In this study, efficiency losses occurring in the combustion chamber during the expansion phase of the piston have been investigated. For this purpose, the boundary conditions of the 2D ring groove cavity CFD model created were derived from the 1D engine model cylinder characteristics. As for the outlet boundary conditions, atmospheric conditions are assumed to be the most ideal situation that causes an increase in leakage flow and pressure loss. Boundary conditions are defined as pressure-based. The boundary conditions used in the model are provided in Table 6.

Table 6. Boundary conditions for the 2D ring cavity CFD model.

Boundary Conditions	Values
Inlet Pressure	3 MPa, 5 MPa, 6.5 MPa
Outlet Pressure	100 kPa
Inlet Temperature	1 888 K
Outlet Temperature	300 K

The CFD model employed a convergence criterion of 10^{-5} and a turbulence intensity of 1%. The SIMPLE (Semi-Implicit Method for Pressure-Linked Equations) Least Squared Cell Based algorithm was utilized for solving the equations. The RANS RNG k-ε turbulence model with standard wall functions and standard initialization was employed as the turbulence model. Additionally, the fluid type used in the model consisted of emission gases with mass ratios entered as multi-phase for theoretical complete combustion, based on the general diesel combustion equation in Equation 12. The emission values obtained according to the reaction in Equation 12, defined as the fluid passing through the ring cavity, and the mass ratios are provided in Table 7.

$$C_{12}H_{23} + 17.75(O_2 + 3.762N_2) \rightarrow 12CO_2 + 11.5H_2O + 66.78N_2 \quad (12)$$

Table 7. Mass fraction of end-combustion emissions fraction of emissions.

Emissions	Mass fraction
CO_2	0.203
H_2O	0.079
N_2	0.718

III.RESULTS AND DISCUSSION

In this study, the efficiency losses in the compression segment cavity of the compression-ignition Renault F8Q706 engine during the expansion phase were investigated using CFD analyses program. The pressure values during the expansion phase (15 degrees after the top dead center) used in the simulations were 3 MPa, 5 MPa, and 6.5 MPa. Compression-ignition engines typically have a high compression ratio, allowing spontaneous combustion in the high-pressure and temperature air-fuel mixture. The combustion results in high pressure, which exerts forces on the cylinder. To ensure the proper functioning of this system, any situation causing pressure loss is undesirable. Combustion, heat transfer, friction, and pumping losses inside the cylinder contribute to efficiency losses. Pumping efficiency during the intake and compression phases is generally around 95% [26]. However, it is also crucial to minimize losses during the expansion phase when power is generated and pressure forces acting on the piston need to be sustained.

The losses occurring in the rings result from two different geometric features. In this study, the flow characteristics in the top compression ring were examined. The investigations were made with CFD analysis, and the resulting graphics consist of the parameters calculated in the analysis. In Figure 8, a comparison of leakage flow is made during the expansion phase for a pressure value of 6.5 MPa obtained from the 1D model and pressures below this value. Generally, with decreasing input pressure due to expansion, the leakage flow and horizontal fluid velocity in the ring groove decrease, while the temperature increases. For pressures of 6.5 MPa, 5 MPa, and 3 MPa, the leakage flows in the ring groove are 2.97E-05, 1.66E-05, and 3.41E-6 kg s-1, respectively. As seen, the decreasing expansion time pressure corresponds to a reduction in leakage flow, reaching 3.41E-6 kg s-1. The decrease in this value with decreasing pressure is expected and normal. These, it leads to less pressure loss. In Figure 9, after compression, a comparison of fluid velocities is made for input pressures of 6.5 MPa, 5 MPa, and 3 MPa obtained from the 1D model. Here, like Figure 8, the highest fluid velocity is calculated at the highest-pressure value. In Table 8, the pressure loss in the ring gaps in response to the expansion stroke pressures taken from the 1D model is given. Here, it is seen that there is more pressure loss with increasing pressure. Considering that the net piston work in the cylinder depends on the in-cylinder pressure in the expansion stroke, it is inevitable that increased pressure loss will cause a decrease in performance in the expansion stroke. Figure 10 presents the fluid's pressure, temperature, and velocity distributions caused by changing input pressures. With decreasing fluid input pressures, there is more restricted fluid entry into the ring groove due to a decrease in leakage flow and, consequently, fluid velocity [7-8]. This has reduced the heat transfer from the fluid to the piston surface, causing a slight increase in the temperature in the ring groove. The small cross-sectional area of the entry and exit sections of the ring groove has led to a pressure increase within the fluid volume, raising the air temperature to 576.47 K. This temperature increase is an expected but undesirable outcome, like the increase in leakage flows.

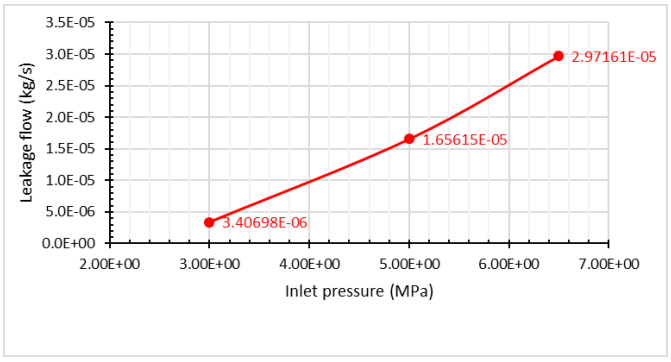

Figure 8. Leakage flows according to inlet pressures.

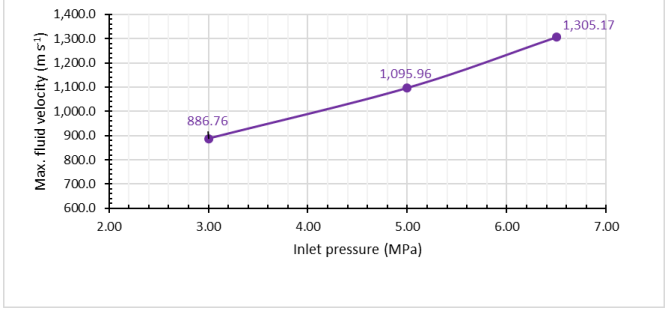

Figure 9. Fluid velocities according to inlet pressures.

Table 8. Performance losses

1B Model in-cylinder pressure, MPa	Pressure loss in CFD, MPa	Net in-cylinder pressure, MPa
3	0.00033	2.99967
5	0.00041	4.99959
6.5	0.00059	6.49941

Figure 10. Pressure, temperature and horizontal velocity contours.

IV.CONCLUSIONS

Studies on the fluid characteristics within the piston ring gaps in reciprocating engines are limited in the literature. Consequently, the ring leakages causing obstacles to the high pressure obtained due to high compression ratios in compression-ignition engines, leading to efficiency losses, have not been thoroughly examined. In this study, the dismantling of the Renault F-Type F8Q706 engine was carried out, and actual cylinder measurements were taken to establish the geometry of the flow volume between the piston and the ring. The engine was initially modeled as 1D, and from there, the temperatures and pressures inside the cylinder during the expansion phase after combustion were calculated. These parameters were then used as boundary conditions for the 2D CFD model of the ring gap. In the 1D model, leakage flows for decreasing pressures of 5 MPa and 3 MPa were also calculated, in addition to the 6.5 MPa pressure obtained at the 15th ATDC (After Top Dead Center) during the expansion phase.

The results obtained from this study provide an interdisciplinary approach where different numerical models are integrated to understand the behavior of the fluid in the ring gap. The findings have the potential to guide the design and optimization processes of the ring in relevant engineering applications related to engines and combustion.

In conclusion, both 1D model and test verifications were conducted, and sensitivity analyses of the 2D CFD model were performed. The behavior of the fluid in the ring gap was extensively examined under the influence of pressure through an integrated approach. The study identified that decreasing pressures led to a reduction in leakage flows.

Nomenclature

Symbols

p	Pressure	1D	1-Dimensional
T	Temperature	3D	3-Dimensional
ρ	Density	RANS	Reynolds-Average Navier-Stokes
c_p	Specific heat	RNG	Re-Normalisation Group (RNG) methods
μ	Viscosity	CO_2	Carbon dioxide
$\dot{\bar{\rho}}^s$	Spray evaporation source term	H_2O	Water
$\dot{\bar{\rho}}^c{}_k$	Chemical reaction source term	CO	Carbon monoxide
$\overline{F}^s$	Momentum gain rate	UHC	Unburned hydrocarbon
DT	Average diffusion coefficient	NO_x	Nitrogen oxides
∇	Gradient vector		
x_b	Flame speed		
θ	Crankshaft angle		

REFERENCES

[1] Türkiye Cumhuriyeti Dışişleri Bakanlığı. (2016). *Paris Anlaşması Metni.* https://www.mfa.gov.tr/paris-anlasmasi.tr.mfa, (12.12.2023).

[2] Türkiye İstatistik Kurumu (TÜİK). (2024). *Motorlu Taşıt İstatistikleri.* https://l24.im/FZoQ, (07.01.2024)

[3] Aktaş, F. (2022). Spark ignition timing effects on a converted diesel engine using natural gas: a numerical study. *Proceedings of the Institution of Mechanical Engineers, Part D: Journal of Automobile Engineering.* 236, 1949-63.

[4] Aktaş, F. (2022). Numerical investigation of equivalence ratio effects on a converted diesel engine using natural gas. *Journal of Energy Resources Technology.* 144, 092305.

[5] Ertugrul, I., Ulkır, O., Ozer, S., Ozel, S. (2022). Analysis of thermal barrier coated pistons in the COMSOL and the effects of their use with water + ethanol doped biodiesel. *Thermal Science.* 26(4A), 2981-2989.

[6] Mohamed, E. S. (2018). Performance analysis and condition monitoring of ICE piston-ring based on combustion and thermal characteristics. *Applied Thermal Engineering*. 132, 824-840.

[7] Hernández-Comas, B., Maestre-Cambronel, D., Pardo-García, C., Fonseca-Vigoya, MDS., Pabón-León, J. (2021). Influence of compression rings on the dynamic characteristics and sealing capacity of the combustion chamber in diesel engines. *Lubricants.* 9(3), 25.

[8] Orozco Lozano, W., Fonseca-Vigoya, MDS., Pabón-León, J. (2021). Study of the kinematics and dynamics of the ring pack of a diesel engine by means of the construction of CFD model in conjunction with mathematical models. *Lubricants*. 9(12), 116.

[9] Koszalka, G. (2019). The use of the gas flow model to improve the design of the piston-rings-cylinder system of a diesel engine. *IOP Conference Series: Materials Science and Engineering.* 659, 012072.

[10] Yeşilada, Ö. (1997). *Piston Rings*. (M.Sc.), Istanbul Technical University, Institute of Science, Department of Mechanical Engineering, Istanbul, Türkiye.
[11] Chucholowski C, Kornprobst H, Zellinger K. (1982). *FVV.* Absclußbericht Nr. 250.
[12] Kornprobst H, Zellinger K. Bewegung, R. (1987). *FVV.* Abschlußbericht Nr. 344.
[13] Furuhama, S. (1959). A dynamic theory of Piston-Ring lubrication: 1st report, calculation, *Bull JSME,* 2, 423-428.
[14] Karamangil, M. E. (2004). Benzinli motorlarda segman ve conta boşluğu hidrokarbonlarının silindir içi dağılımı, *Uludağ Üniversitesi Mühendislik-Mimarlık Fakültesi Dergisi*, 9(1), 53-64.
[15] Lyubarskyy, P., Bartel, D. (2016). 2D CFD-model of the piston assembly in a diesel engine for the analysis of piston ring dynamics, mass transport and friction, *Tribology International, 104, 352-368.*
[16] Satge´ de Caro, P., Mouloungui, Z., Vaitilingom, G., Berge, J. C. (2001). Interest of combining an additive with diesel–ethanol blends for use in diesel engines. *Fuel*. 80(4), 565-574.
[17] Woschni, G. (1967). A universally applicable equation for the instantaneous heat transfer coefficient in the internal combustion engine. *SAE Int.* J. *Engines.*
[18] Ghojel, J. I. (2010). Review of the development and applications of the wiebe function: a tribute to the contribution of Ivan Wiebe to engine research. *International Journal of Engine Research*. 11(4), 297-312.
[19] Wiebe, I. (1956). *Semi-empirical expression for combustion rate in engines*. InProceedings of Conference on Piston Engines.
[20] Newhall, H. K. (1969). *Kinetics of engine-generated nitrogen oxides and carbon monoxide*. Symposium (International) on Combustion. 12(1), 603-613.
[21] Cheng, W. K., Hamrin, D., Heywood, J. B., Hochgreb, S., Min, K., Norris, M. (1993). An overview of hydrocarbon emissions mechanisms in spark-ignition engines. *SAE Int. J. Engines*.
[22] Fenimore, C. P. (1971). *Formation of nitric oxide in premixed hydrocarbon flames*. Symposium (International) on Combustion. 13(1), 373-380.
[23] Pipitone, E. (2009). A new simple friction model for s. i. engine. *SAE Technical Paper*.
[24] Özer, S. (2014). Alkollerin içten yanmalı motorlarda alternatif yakıt olarak kullanılması. *Uludağ Üniversitesi Mühendislik-Mimarlık Fakültesi Dergisi, 19(1),* 97-114.
[25] Aktaş, F. (2021). *Numerical investigation of the effects of the use of propane-diesel as a dual fuel in a diesel engine on the combustion regime, engine performance and emission values*. (PhD), Gazi University, Ankara, Türkiye.
[26] Heywood, J. B. (1988). *Internal Combustion Engine Fundamentals*. McGraw-Hill.
[27] Mahle GmbH. (2012). *Pistons And Engine Testing* (1st ed). Vieweg – Teubner.
[28] Winterbone, D. E., Turan, A. (2015). *Advanced Thermodynamics For Engineers* (2nd ed). Butterworth-Heinemann an Imprint of Elsevier.
[29] Engine catalog. (2021). https://mymotorlist.com/engines/renault/, (12.12.2023).